

# 1 **Assessing flooding impact to riverine bridges: an integrated analysis**

2 Maria Pregnolato<sup>1\*</sup>, Andrew O. Winter<sup>2</sup>, Dakota Mascarenas<sup>2</sup>, Andrew D. Sen<sup>3</sup>, Paul Bates<sup>4</sup>, Michael R.  
3 Motley<sup>2</sup>

4 <sup>1</sup> Dep. of Civil Engineering, University of Bristol, Bristol, BS8 1TR, UK

5 <sup>2</sup>Dep. of Civil and Environmental Engineering, University of Washington, Seattle, 98103, USA

6 <sup>3</sup>Dep. of Civil, Construction and Environmental Engineering, Marquette University, Milwaukee, 53233, USA

7 <sup>4</sup>School of Geographical Sciences, University of Bristol, Bristol, BS8 1RL, UK

8 \*Correspondence to: Maria Pregnolato (maria.pregnolato@bristol.ac.uk)

9 **Abstract.** Flood events are the most frequent cause of damage to infrastructure compared to any other natural hazard, and  
10 global changes (climate, socio-economic, technological) are likely to increase this damage. Transportation infrastructure  
11 systems are responsible for moving people, goods, and services, and ensuring connection within and among urban areas. A  
12 failed link in this system can impact the community by threatening evacuation capability, recovery operations and the overall  
13 economy. Bridges are critical links in the wider urban system since they are associated with little redundancy and a high  
14 (re)construction cost. Riverine bridges are particularly prone to failure during flood events; in fact, the risks to bridges from  
15 high river flows and bank erosion have been recognized as crucial at global level. The interaction among flow, structure and  
16 network is complex, and not fully understood. This study aims to establish a rigorous, multiphysics modelling approach for  
17 the hydrodynamic forces impacting inundated bridges, and the subsequent structural response, while understanding of the  
18 consequences of such impact on the surrounding network. Objectives of this study are to model hydrodynamic forces as  
19 demand on the bridge structure, to advance a performance evaluation of the structure under the modelled loading, and to assess  
20 the overall impact at systemic level. The flood-prone City of Carlisle (UK) is used as case study and a proof of concept.  
21 Implications of the hydrodynamic impact on the performance and functionality of the surrounding transport network are  
22 discussed. This research will help to fill the gap between current guidance for design and assessment of bridges within the  
23 overall transport system.

## 24 **1 Introduction**

25 Bridges are crucial elements of the transport network given their high construction costs and the lack of alternatives routes.  
26 Man-made and natural events are a threat to bridge safety and network serviceability (Yang and Frangopol, 2020). Bridges act  
27 as bottlenecks for surrounding roads, and thus any service disruption can knock-out communities' access and connections,  
28 impair emergency planning and evacuation routes, as well as impact economies and businesses.

29 Some disruptive events are growing in frequency and severity. In particular, the impacts of flooding have been exacerbated in  
30 recent years by urbanisation (e.g. increase of impermeable surfaces), inappropriate land use in flood-prone areas and climate  
31 change. Rainfall events that lead to flooding are becoming more frequent and intense (Solomon et al., 2007), triggering bridge  
32 incidents and failures all over the world (Cumbria, UK, 2009; Drake, Colorado, 2013; Texas, 2018; Greece, 2020). As recent  
33 examples, Grinton Bridge in Yorkshire (North-West UK) and Keritis Bridge in Crete (Greece) were both washed away by  
34 floodwaters in 2019.

35 Riverine bridges are intrinsically vulnerable to flooding, as they are located in the area of the riverbed. Flood and scour  
36 represent the most frequent cause of bridge failures (>50% of all failures; Wardhana and Hadipriono, 2003; Ahamed et al.,  
37 2020). Although, scour is recognized as the biggest threat, the available literature related to scour is much more robust, and  
38 hydrodynamic forces could be as critical for bridge piers on bedrock (where scour is unlikely), and for the decks of all flooded  
39 bridges (Kim et al., 2017; Oudenbroek et al., 2018). In terms of consequences, natural hazards can damage bridges structurally  
40 (thus causing direct physical damages), but these events can also result in functional failures that cause travel time delays and

41 rerouting that lead to indirect losses. Any bridge failure, whether structural or functional, has the potential to impose heavy  
42 consequences to owners or responsible authorities, as well as dire expenses. Therefore, understanding the potential impact of  
43 flooding to bridges is a compelling need of communities in areas of high flood risk.  
44 Currently, a limited number of studies investigated the consequences of extreme flooding to bridges and the surrounding  
45 network (Yang and Frangopol, 2020). Practical application and case studies of real bridges tend to be focused on other natural  
46 hazards (e.g. earthquakes: Kilanitis and Sextos, 2019, Ertugay et al., 2016; Zhou et al., 2010). This study aims to establish a  
47 rigorous, multiphysics modelling approach for the hydrodynamic forces on inundated bridges, subsequent structural response,  
48 and understanding of the consequences of such impact on the surrounding network. Objectives of this study are to model  
49 hydrodynamic forces as demand on the bridge structure, to advance a performance evaluation of the structure under the  
50 modelled loading, and to assess the overall impact at systemic level. Implications of the hydrodynamic impact on the  
51 performance and functionality of the surrounding transport network are discussed. This research will help to fill the gap  
52 between current guidance for design and assessment of bridges within the overall transport system.

### 53 **1.1 Background**

54 Transport networks are formed by multiple links (i.e. roads), and their performance relies on a number of parameters, such as  
55 availability of alternative routes (redundancy), road capacity, or traffic demand, among others. A bridge failure often means a  
56 critical link been taken out of service. Bridges are usually costly assets to be repaired, have little redundancy and are likely to  
57 be crossed by a high number of users, especially if belonging to strategic road networks (e.g. highways). Therefore, bridge  
58 closure or failure can impact the overall performance of the road network and the failure consequences have to be investigated  
59 from a system-perspective (Yang and Frangopol, 2020). The assessment of the systemic impact is a complex and multi-  
60 disciplinary problem, at the interface of hydrology, fluid dynamics, structural analysis and transport modelling.

61 Scour damage is a significant concern for bridge structures and has been studied in much detail (e.g. Pregnotato et al., 2021a;  
62 Wang et al., 2017; Hung and Yau, 2017; AASHTO, 2002), however it is not the main focus of this paper. On the contrary,  
63 literature about modeling the hydrodynamic forces of the fluid on bridges due to riverine floods is limited, especially  
64 concerning fragility models or reliability analysis (Pregnotato, 2019; Gidaris et al., 2017). Existing research investigated  
65 tsunami impact to bridges (e.g. Motley and al., 2016; Lomonaco et al., 2018; Qin et al., 2018; Winter et al., 2017), where  
66 Computational Fluid Dynamics (CFD) techniques are used to compute hydrodynamic forces on bridges and components. Also,  
67 Kerényi et al. (2009) applied CFD to compute hydrodynamic forces on inundated bridge decks, however the analysis was  
68 limited to the evaluation of drag and lift forces, without investigating impact and consequences. Multi-hazard studies have  
69 investigated the interaction and implication of multiple hazards acting on a single structure (Gidaris et al., 2017; Carey et al.,  
70 2019), especially between earthquake and tsunami. Other studies (Mondoro and Frangopol, 2018; Liu et al., 2018; Yilmaz et  
71 al., 2016) that tackled flood impact to bridges generally expressed the hazard through flood hazard curves, generated via flood-  
72 frequency analysis; however, a detailed hydraulic analysis was beyond the scope of their work. While tsunami loading of  
73 bridges will often result in much higher forces than riverine flows, the prevalence of riverine flooding relative to tsunami  
74 events necessitate further study and could have a far-reaching effect.

### 75 **1.2 Motivation and aim**

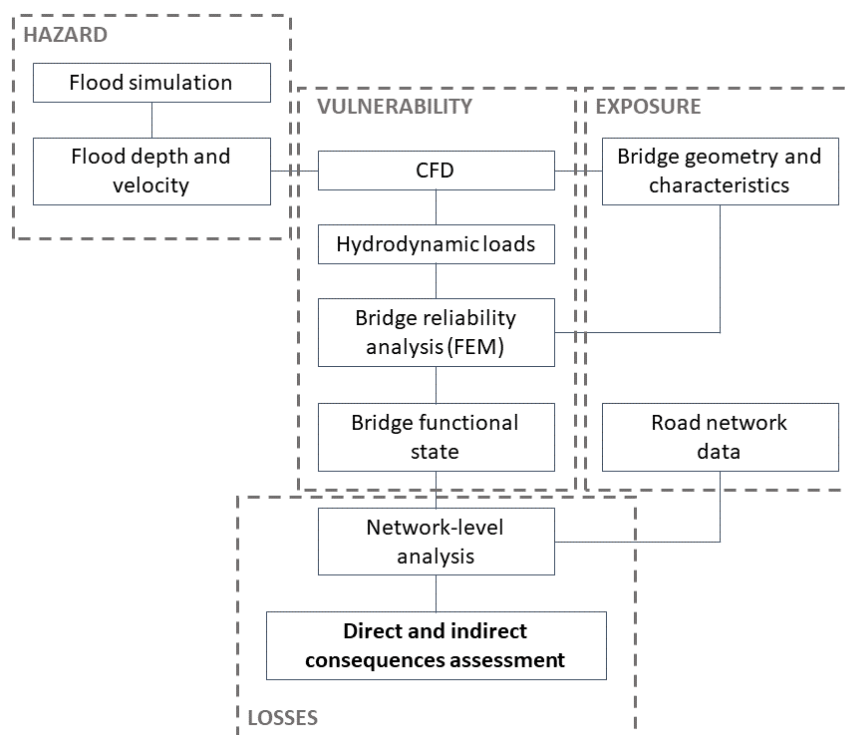
76 To the authors' knowledge, no study has comprehensively investigated the impact of high-river flows on bridges accounting  
77 for the complexity of the hydrodynamic forces to which the bridge is subjected and the associated structural and functional  
78 response. Moreover, the impact of the reduced service on a bridge on the surrounding network is rarely addressed in literature.  
79 Given this limited availability of models, this paper aims to establish a multilevel modeling framework to address these issues  
80 in one combined approach. This aim is achieved by developing an integrated framework to assess the flooding impact on  
81 riverine bridges from the structural- to the network-level (Pregnotato et al., 2021b) and applying it to a real case study in the

82 UK. This research tackles varying flow conditions (velocity and depth) to understand the structural response across given  
 83 simulated flooding conditions. This work is novel since it represents a first attempt to couple CFD analysis with both Finite  
 84 Element (FE) and network analysis for bridges subjected to flooding, in an effort to capture both the cause and effect of  
 85 flooding. It is expected that this approach will be useful for understanding structural damage and functional loss for a range of  
 86 bridges, and ultimately to assess risk for any coastal or riverine structure where large-scale water inundation is expected.

## 87 2 Method

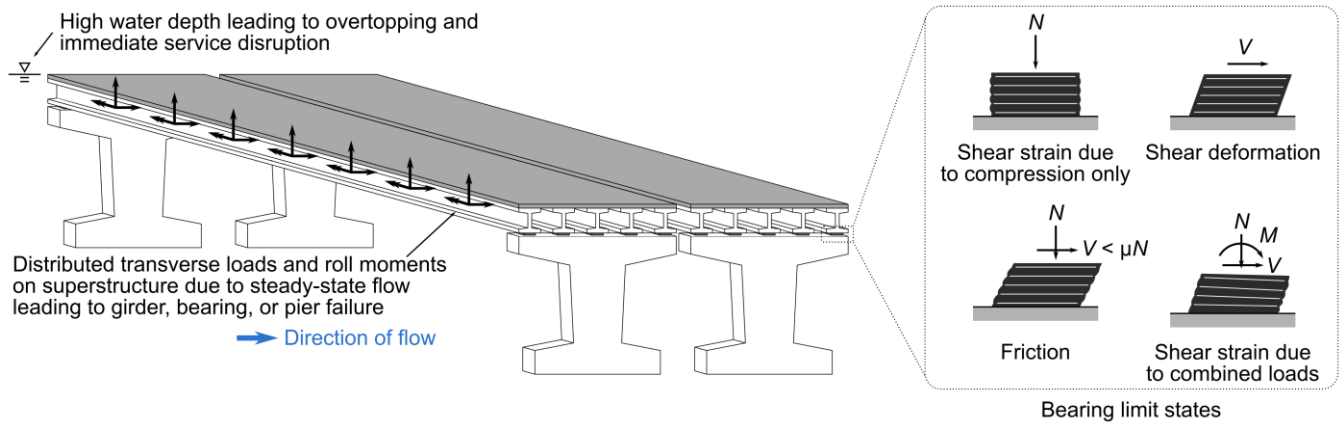
88 This paper adopts a risk-based framework to assess the impact of high river flows to bridges and surrounding roads (Figure 1).  
 89 The framework proposes a comprehensive method that encompasses the traditional four risk modules (hazard, exposure,  
 90 vulnerability and consequences; Grossi and Kunreuther, 2005) and includes hydrodynamic force modelling, bridge  
 91 susceptibility to the hazard, performance evaluation and network-level impact assessment. This study adopts specific  
 92 models/software, but the precise sub-models chosen are not critical. In fact, all models/software are interchangeable, and it is  
 93 reasonable to expect that the approach presented would be appropriate for software packages that ensure similar configuration.  
 94 The first step is to determine the intensity measures of flooding in terms of flow depth and velocity (see Section 2.1). For  
 95 modelling fluvial flooding, most 2D hydrodynamic models can simulate flood depths and flow velocity, e.g. *LISFLOOD-FP*  
 96 (<https://bit.ly/3lstd4j>) or *TELEMAC* (<http://www.opentelemac.org/>). Bridge information, such as geometry and design, can be  
 97 retrieved through publicly available databases (e.g. the US National Bridge Inventory) or by coordination with local  
 98 infrastructure managers and authorities to determine parameters including but not limited to bridge dimensions, number of  
 99 piers, material, design principle, foundation type. Unsurprisingly, the availability and accuracy of data vary from bridge to  
 100 bridge and can influence the modelling outputs.

101 The second step consists of modelling the interaction between the water and the bridge, as well as the subsequent flood-induced  
 102 loads. The local flow conditions and corresponding hydrodynamic forces that represent the load on the bridge structure are  
 103 evaluated using Computational Fluid Dynamics (CFD) techniques. Here, the C++ toolbox *OpenFOAM* is the adopted software,  
 104 being open-source and particularly versatile for the development of customized numerical solvers  
 105 (<https://www.openfoam.org/>).



107 **Figure 1: The proposed risk-based methodological flowchart to integrate modelling of hydrodynamic forces, performance and**  
108 **network-level analysis. Acronyms: CFD - Computational Fluid Dynamics; FEM – Finite Element Model.**

109 The third step is to determine the response of the bridge subjected to flood through an advanced structural analysis approach  
110 such as Finite Element (FE) analysis. There are many available FE models, such as Abaqus FEA ([www.3ds.com](http://www.3ds.com)), ANSYS  
111 (<https://www.ansys.com/en-gb>), SAP2000 (<https://www.csiamerica.com/products/sap2000>) or the *OpenSees* software  
112 framework (McKenna et al., 2010). Mondoro and Frangopol (2018) described salient limit states for bridges subjected to  
113 hydraulic loads, and the subset studied in this paper (shown in Figure 2) includes yielding of the girders or piers, unseating or  
114 uplift of the girders, failure of the bearings, and excessive global displacement of the superstructure at which transient fluid-  
115 structure interaction is important (i.e., the CFD modeling approach is limited).



116

117 **Figure 2: Bridge failure states investigated due to flood loading.**

118 The general limit-states philosophy considers that specifications should satisfy “specified limit states to achieve the objectives  
119 of constructability, safety and serviceability” (AASHTO, 2017). In this work, the failure of a bridge is seen as twofold: (i)  
120 structural (also strength limit state), when the bridge deck, piers or foundation reach the ultimate limit state or permanent  
121 deformations; (ii) functional (also service limit state), when the bridge cannot perform its service as usual. A structural failure  
122 directly leads to a functional failure, e.g. the bridge collapses; preventive closure could also take place when bridge conditions  
123 are considered unsafe. Nevertheless, a bridge could be unserviceable but still structurally sound, e.g. when floodwater or debris  
124 cover the deck. Hydraulic pressures (drag, lift and overturning moment) are assessed for potentially dislodging the deck from  
125 piers, when submerged or partially sub-merged, and overtopping of the deck is evaluated qualitatively from the CFD model.  
126 Though these limit states have significantly different long-term consequences, both result in potential functional failure. The  
127 importance of long-term effects should be defined based on local transportation needs.

128 The last step is to assess consequences, by including the impact of the bridge failure on the wider transport network. Transport  
129 models such as *ESRI™ ArcGIS Network Analyst* (<https://bit.ly/2GPMknl>), *SUMO* (<http://sumo.sourceforge.net/>) or *MatSIM*  
130 (<https://www.matsim.org/>) are suitable for computing routing and delays associated with a disrupted network link (such as a  
131 closed bridge). Road network data are publicly available from sources such as Digimap® (<https://digimap.edina.ac.uk/>), which  
132 provides Ordnance Survey road maps. These contain topographic information of roads including name, location, length,  
133 capacity and type. After configuring the transportation network model with the collected data, routing and accessibility can be  
134 investigated using network-based spatial analysis and transport appraisal techniques (Arrighi et al., 2020; Pregnotato et al.,  
135 2016). This impact analysis links the structural damage of a bridge due to flooding with the reduced performance of the local  
136 road network the bridge serves for, approximating the wider consequences.

## 137 2.1 Fluvial flooding simulation

138 Ideally, boundary conditions should be provided by gauging stations; however, no river gauges are present near the bridge of  
139 interest, as is often the case in practical scenarios. This study adopted the 2D hydrodynamic model *LISFLOOD-FP*, which

140 allows to simulate flood depths and flow velocity to set up CFD boundary conditions for a flood scenario and from available  
141 gauge data.

142 *LISFLOOD-FP* is a two-dimensional, spatially distributed, grid-based hydrodynamic model for simulating channel and  
143 floodplain flows (Neal et al., 2009). The model dynamically simulates flood propagation in each grid cell at each time step, on  
144 the basis of the local inertial formulation of the shallow water equations and an explicit finite difference method. Numerically,  
145 this process involves calculating the momentum equation (the flow between cells given the mass in each cell) and the continuity  
146 equation (the change in mass in each cell given the flows between cells) (Neal et al., 2018). The equations underpinning the  
147 model, including their derivation, can be found in Bates et al. (2010) and de Almeida et al. (2012).

148 As input data, *LISFLOOD-FP* requires a DEM (Digital Elevation Model) of the area, channel and boundary condition  
149 information (e.g. channel friction, width and depth, hydrograph and evaporation). Flow depth and velocity (for each cell) are  
150 the output considered, since they represent the intensity measures of the hazard adopted by this study. The impact of bridges  
151 on flow is not explicitly represented in this particular application.

## 152 **2.2 Computational fluid dynamics (CFD) analysis**

153 Three-dimensional (3D) CFD software is capable of resolving fine details of flood flow around bridges on a local scale such  
154 as splashes, eddies, or flow separation, which cannot be captured by depth-averaged methods (such as *LISFLOOD-LP*). Also,  
155 bridges present a problem for depth-averaged tools since the computational mesh is two-dimensional and cannot be discretized  
156 vertically, which does not allow for a gap underneath a bridge superstructure. To accurately model such behaviors is crucial  
157 when estimating flow-induced force demands, which requires the use of a fine, three-dimensional mesh. Additionally, using  
158 higher fidelity, three-dimensional models allow for localized loads to be measured on individual faces of a structure, which  
159 may be used to determine whether or not individual components fail versus entire structures (Winter et al., 2017).

160 For this study, the three-dimensional CFD code *OpenFOAM* was selected. Flood flows were modelled using the *interFoam*  
161 solver, which is a two-phase solver that relies upon Volume of Fluid (VoF) method (Tryggvason et al., 2011) to track the  
162 interface between water and air phases. The underlying governing equations that are implemented in *interFoam* are the  
163 Reynolds-averaged Navier-Stokes (RANS) equations, which are solved using a predictor-corrector or projection type of  
164 method to solve for velocity and pressure fields, and advection equations for the volume fraction introduced by the VoF  
165 method. More specifically, pressure-velocity coupling was achieved using the PIMPLE algorithm, which is a combination of  
166 the Pressure-Implicit Split-Operator (PISO) and Semi-Implicit Method For Pressure-Linked Equations (SIMPLE). Since the  
167 RANS system of equations does not constitute a well-posed system due to the so-called Reynolds stress tensor that arises from  
168 the Reynolds-averaging process, a suitable turbulence model that introduces additional equations must be chosen to close the  
169 system. For this study, the  $k-\omega$  Shear Stress Transport (SST) model was used due to its ability to handle severely separated  
170 flows near sharp corners better than other similar models such as the Standard, Renormalization Group (RNG), or realizable  
171  $k-\epsilon$  models.

## 172 **2.3 Structural analysis**

173 At a minimum, the structural analysis approach used should be capable of (i) simulating relevant structural response  
174 mechanisms, which differ based on bridge type, and (ii) characterizing loading derived from the associated CFD model. Finite  
175 element (FE) analysis is commonly employed in structural engineering to simulate the response of bridges to natural hazards  
176 for the purpose of design and performance evaluation. Modern reinforced concrete and steel bridge structures are commonly  
177 formed of girders, cap beams, and pier walls or columns which can be modeled as assemblages of line and spring elements;  
178 this approach is common in practice and can be implemented in a wide variety of structural analysis programs. To model  
179 nonlinear response, which is especially important when considering extreme loads associated with natural hazards, line  
180 elements may employ concentrated or distributed plasticity formulations that make use of nonlinear hinges or fiber sections.

181 Rotational, shear, and/or axial spring elements can be used to simulate the response of discrete components such as connections  
182 and bearings. Alternatively, continuum finite-element analysis can be employed for members if complex local response of  
183 components (e.g. local buckling and/or deformation) is of interest; this approach is significantly more computationally  
184 expensive, however. Other approaches, such as the discrete-element method, may be well suited for masonry bridges.  
185 In this work, modeling with line and spring elements is performed, so this approach will be discussed in greater detail. The  
186 case study bridge consists of a girder superstructure supported on reinforced concrete piers. *OpenSees* (McKenna et al. 2010)  
187 was selected as the analysis software due to its robust nonlinear modeling and scripting capabilities. This latter capability is  
188 beneficial for performance evaluation using a suite of input parameters (in this case, a parameter sweep characterizing different  
189 flood conditions). Moreover, the software is open source and therefore suitable for adaptation in envisioned future work to  
190 enhance interactivity with *OpenFOAM*.  
191 Component response and demands based on the structural analysis can be used to assign a damage state for the bridge. Here,  
192 the structural damage is evaluated as slight, moderate, extensive, or complete damage based on the FEMA Hazus manual  
193 (FEMA, 2003). Each of these damage states is associated with level of functionality and repair effort. The qualitative  
194 description of damage states and average repair cost per m<sup>2</sup> (ft<sup>2</sup>) is available in literature for hurricanes (Padgett et al., 2008)  
195 and earthquakes (Hazus manual - FEMA, 2003); Gehl and D’Ayala (2018) offered a qualitative damage scale of potential  
196 damage state and failure modes for the bridge components, which could be associated with functionality losses and remedial  
197 actions. Table 1 adapts such literature to riverine flooding using these works and expert opinion: it lists four identified damage  
198 states (from slight to complete), and associated average repair cost and days of closure due to remedial works (Werner et al.,  
199 2008; Gardoni, 2018; Lam and Adey, 2016).

200 **Table 1. Bridge damage states (Gehl and D’Ayala, 2018) associated to average repair cost per m<sup>2</sup> (Padgett et al., 2008; FEMA, 2003)**  
201 **and average days of closure due to repair (Werner et al., 2008; Gardoni, 2018; Lam and Adey, 2016).**

Damage state	Description	Average repair cost (£/m <sup>2</sup> )	Days of closure
Slight	Minor damages such as cracking (shear keys, hinges, deck) and spalling (hinges, columns) that require no more than cosmetic repair. Negligible scour. Some water and/or debris on deck. Full service, likely speed reduction of travelling vehicles.	£1.45/m <sup>2</sup> (\$0.25/ ft <sup>2</sup> )	0-5
Moderate	Moderate experience of shear cracks and spalling that still leave columns structurally sound. Moderate scour and moderate movement of the abutments. Significant water and/or debris on deck. The bridge is partially serviceable (e.g. alternating circulation, reduced capacity and load), but safe to use by emergency vehicles.	£36.54/m <sup>2</sup> (\$6.28/ ft <sup>2</sup> )	5-12
Extensive	Degradation of columns without collapse, shear and cracking leading to structurally unsafety. Significant residual movement at connections or major settlement approach. Delamination failure of individual bearings.	£308.66/m <sup>2</sup> (\$53.05/ ft <sup>2</sup> )	13-49

	Extensive scour of abutments. The bridge is closed to traffic.		
Complete	Collapse of columns or connection losing all bearing support. Imminent deck collapse. Unseating of girders. Scour leading to foundation failure. The bridge is unserviceable.	£1102.77/m <sup>2</sup> (\$189.43/ft <sup>2</sup> )	>50

202

## 203 2.4 Fluid-structure coupling

204 The relationship between the CFD and structural analysis is critical to implementation of the proposed framework as outlined  
 205 in the vulnerability analysis block in Figure 1. Both analyses must adequately represent the bridge geometry, and the CFD  
 206 output and structural analysis input loading must be compatible. Here, the coupling approach between *OpenFOAM* and  
 207 *OpenSees* is discussed, but the methodology is applicable to other software. It is noted that *OpenSees* alone is seldom used to  
 208 model structural response to fluids because of the complexity of the fluid loading and the required coupling mechanism  
 209 between fluid and solid solvers. As such, the present work is among the first of its kind using *OpenSees*. Other recent research  
 210 has sought to implement coupling between these multi-physics models. For example, Stephens et al. (2017) demonstrated how  
 211 *OpenSees* can be “loosely coupled” (i.e., with no interaction between CFD and FE models) with *OpenFOAM* to characterize  
 212 structural response due to sequential earthquake and tsunami loading. A similar loosely coupled scheme is used here, where:

- 213 i. the bridge superstructure (deck and girders) is modeled as a rigid, 2D cross section with a unit length out of plane and  
 214 subjected to steady-state flow at different water depths and velocities in *OpenFOAM*;
- 215 ii. the steady-state reactions (output from *OpenFOAM*) on the cross section are recorded; and
- 216 iii. the gravity loads and the steady-state reactions from *OpenFOAM* are applied as distributed, external loads on girder  
 217 line elements in a 3D *OpenSees* model of the full bridge.

218 It is noted that the bridge superstructure is rigid in the computational fluid dynamics model (an important simplification to  
 219 facilitate the analysis) but not in the finite-element model.

## 220 2.5 Impact assessment

221 The impact of a bridge failure in terms of consequences ( $C$ ) includes direct consequences ( $C_{dir}$ ) and indirect consequences  
 222 ( $C_{ind}$ ), which relate the surrounding transport network (Argyroudis et al., 2019). The total costs  $C$  is computed as (Eq. 1):

$$C = C_{dir} + C_{ind} = C_{repair} + C_{cleaning} + C_{detour} + C_{delay} \quad \text{Eq. 1}$$

223 where  $C_{repair}$  is the cost associated with repair or replacement of the bridge,  $C_{clean}$  is the cost associated with the debris removal  
 224 (due to flooding),  $C_{detour}$  is the additional vehicle operating due to the detour and  $C_{delay}$  is the cost associated with trip delays of  
 225 normal traffic. Indirect costs may also include a fee for closing the bridge that the bridge owner has to pay to transport  
 226 operators/agencies (e.g. for railways, highways).

227 Table 1 (Sec. 2.3) was functional to compute  $C_{repair}$ . Average days of closure due to repairs are obtained via discussion with  
 228 national operators and existing literature (Werner et al., 2008; Gardoni, 2018; Lam and Adey, 2016). Values for  $C_{clean}$  can be  
 229 researched among historic data of bridge owners, e.g. records from bridge inspection reports.  $C_{detour}$  and  $C_{delay}$  depend on the  
 230 network, type of vehicle and traffic flow; this study is limited to consider private cars and HGVs (Heavy Goods Vehicles, i.e.  
 231 over-3.5-tonnes-gross vehicle weight, including both articulated and rigid body types), for the sake of a contained  
 232 demonstration. According to standard transport appraisal procedures (e.g. DfT, 2009), the parameters are computed with Eq.  
 233 2 and Eq. 3 respectively. Considering an origin  $i$ , a destination  $j$  and a vehicle type  $z$ :

234



$$C_{detour} = \sum_i \sum_j \sum_z q_{i,j,z} l_{i,j,z} VOC_z \quad \text{Eq. 2}$$

$$C_{delay} = \sum_i \sum_j \sum_z q_{i,j,z} d_{i,j,z} VTT_z \quad \text{Eq. 3}$$

235

236  $q$  is the volume of traffic,  $l$  is the incurred additional length,  $d$  is the incurred additional time (delay),  $VOC$  is the extra Vehicle  
 237 Operating Cost (including fuel, tear and wear) and  $VTT$  is the Value of Travel Time, i.e. the non-monetary costs incurred along  
 238 the journey as time spent on transport. The additional length and travel time due to the detour are computed using *ESRI*<sup>TM</sup>  
 239 *ArcGIS Network Analyst*, setting the origin and the destination of the trip in opposite sides of the river as demonstration  
 240 (Pregolato et al., 2016).

### 241 3 Application and results

242 The City of Carlisle is a flood-prone city (area: 1,040 km<sup>2</sup>; 2018 population: 108,387) located in the North West of England  
 243 (UK) (Figure 3). Three road bridges connect the two parts of the town over the river Eden from North to South (the A689, A7  
 244 and M6 bridges) and a fourth one from West to East (Warwick bridge). The 2D hydrodynamic model *LISFLOOD-LP* was set  
 245 up to simulate a 1-in-500-year flooding scenario (Fig. 3b) for a domain covering 14.75 km<sup>2</sup> of Carlisle, at 5 m of resolution.  
 246 This simulation provided flow velocity and inundation height data.

247 As a proof of concept, the M6 highway bridge over the River Eden was considered. The bridge is comprised of a girder

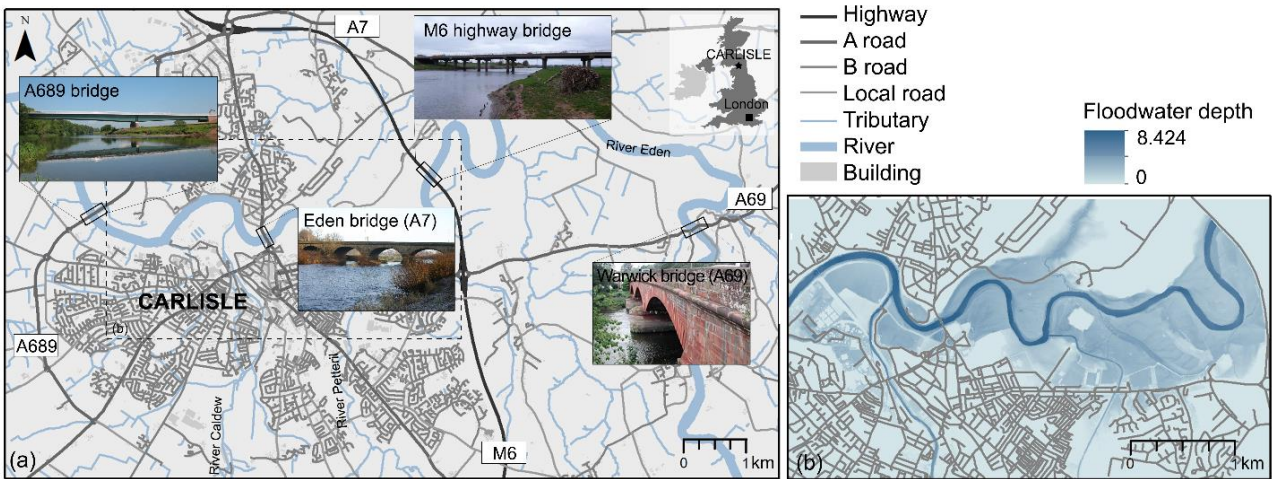
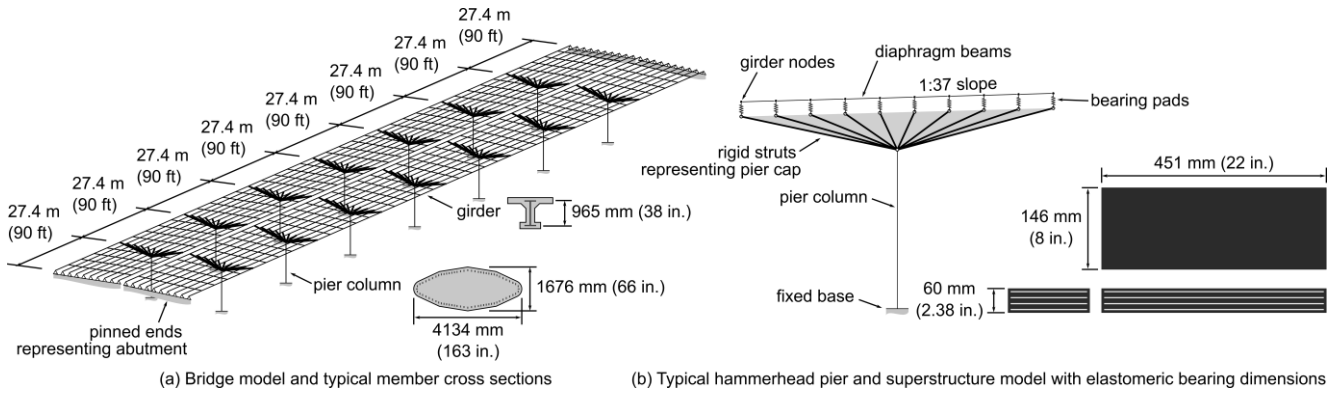


**Figure 3. The case study is the city of Carlisle, UK: (a) general overview of Carlisle upon the river Eden, connected North-South by three road bridges (the A689, A7 and M6 bridges) and West-East by the Warwick bridge (A69); (b) flood hazard map for Carlisle, as simulated with LISFLOOD-LP for a 1-in-500-year flood event.**

248 superstructure supported by hammerhead piers. A schematic model of this bridge is shown in Figure 4 with approximate pier  
 249 column (reinforced concrete), girder (concrete-encased steel), and bearing pad dimensions. The pier columns are elliptically  
 250 shaped and oriented to reduce hydraulic drag. The columns taper to a width of 4134 mm and depth of 1676 mm at the base.  
 251 The girders are supported on fixed, laminated elastomeric bearing pads with dowels at the southern end of each span and free  
 252 spherical bearings at the northern end. Salient bridge and flow input data are summarized in Table 2.

253





254 (a) Bridge model and typical member cross sections (b) Typical hammerhead pier and superstructure model with elastomeric bearing dimensions

255 **Figure 4. Approximate geometry of M6 bridge as modeled in *OpenSees* including pier column, girder, and bearing dimensions shown**  
 256 **(not to scale).**

257 **Table 2. Input data of this study for the exemplary CFD analysis of the M6 bridge (Carlisle, UK).**

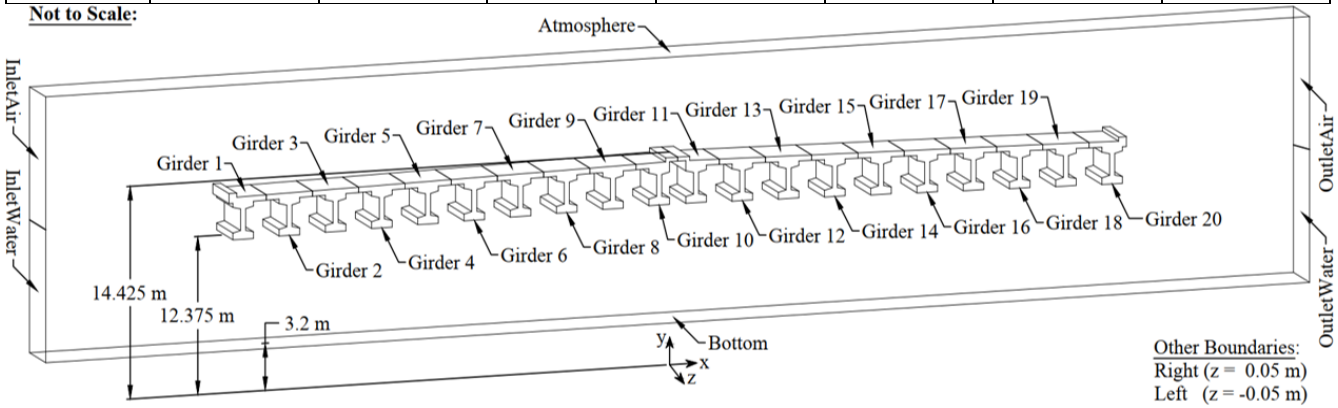
VARIABLE	DATA	SOURCE
Span length	27.4 m	Drawings provided by Highways England
Pier width	17.1 m	Drawings provided by Highways England
Superstructure weight (deck, girders, and diaphragm beams)	514 kN/m	Derived from drawings
Flow Velocity	1, 2, and 3 m/s	Modelled (LISFLOOD-LP)
Inundation Height	12.5, 13.0, 13.5, 14.0, 14.5, 15.0, 16.0, 17.0, 18.0 m (from datum; +3.2 m)	Modelled (LISFLOOD-LP)

258  
 259 The CFD simulation was initiated at given inundation heights and flow velocity, as modelled by the *LISFLOOD-LP* model for  
 260 a 1-in-a-500-year flood event at the site. The *OpenFOAM* model was set to simulate a range of flow velocity and depth values  
 261 above and below the calculated 500-year flood results in order to assess how varying the depth and velocity affected the  
 262 resulting bridge performance. Flow velocities and depths were extracted from LISFLOOD-LP in proximity of the bridge, and  
 263 also compared with historical data overall (e.g., the peak flow recorded at Sheepmount, UK in December 2015 was equal to  
 264 1680.0 m<sup>3</sup>/s; EA, 2016) and inspection reports. The statistics for the velocity (both in its actual flood flow direction and also  
 265 normal to the bridge) were computed from the *LISFLOOD-LP* velocity vector ( $V_x$ ,  $V_y$ ) and maximum water depth data,  
 266 considering maximum values for both quantities over the whole flood simulation. The 500-year return period flood showed  
 267 velocity values up to roughly 3.5 m/s and max flood depth up to 17 m near the M6 Bridge. These statistics motivated using a  
 268 range of steady-state velocities of 1-3 m/s and inundation elevations of 12.5-18 m above datum in the *OpenFOAM* simulations.  
 269 The bridge superstructure was positioned such that the bottom of the bridge's lowest girders and the highest point of the top  
 270 of the bridge deck were at elevations of 12.375 m and 14.425 m, respectively, relative to the datum, which was 3.2 m below  
 271 the riverbed's lowest point. Flow rates corresponding to the range of selected flow velocities and depths were specified at the  
 272 inlet boundary of the *OpenFOAM* model. A full summary of all *OpenFOAM* boundary conditions is provided in Table 3. To  
 273 reduce computation time and provide conservative results, a unit width segment of the bridge superstructure located above the  
 274 deepest point of the Eden River beneath the M6 Bridge was analyzed in *OpenFOAM*, which resulted in a 2D simulation that  
 275 drastically reduced the mesh cell count compared to a full 3D simulation of the entire bridge. Additionally, the out-of-plane  
 276 direction components of the flow were neglected in all simulations by using the empty type of *OpenFOAM* boundary condition,  
 277 ensuring the simulations were truly 2D. This setting allowed for more simulations to be run using a wider range of flooding  
 278 conditions in less time while conducting the parametric study. As shown in Fig. 5, the model measured forces on 20 individual

279 components along the cross-section of the bridge superstructure segment corresponding to each girder and its tributary width  
 280 of the bridge deck.

281 **Table 3. OpenFOAM model boundary conditions.**

Boundary	OpenFOAM Simulation Field Variables						
	alpha	epsilon	k	nut	omega	p_rgh	U
InletWater	variableHeight-Flowate	fixedValue	fixedValue	calculated	fixedValue	zeroGradient	variableHeightFlow-RateInletVelocity
InletAir	inletOutlet	inletOutlet	inletOutlet	calculated	inletOutlet	totalPressure	pressureInletOutlet-Velocity
OutletWater	zeroGradient	zeroGradient	zeroGradient	calculated	zeroGradient	zeroGradient	inletOutlet
OutletAir	zeroGradient	zeroGradient	zeroGradient	calculated	zeroGradient	totalPressure	pressureInletOutlet-Velocity
Right	empty	empty	empty	empty	empty	empty	empty
Left	empty	empty	empty	empty	empty	empty	empty
Bottom	zeroGradient	epsilonWall-Function	kqRWall-Function	nutkWall-Function	omegaWall-Function	fixedFlux-Pressure	noSlip
Atmosphere	inletOutlet	inletOutlet	inletOutlet	calculated	inletOutlet	totalPressure	pressureInletOutlet-Velocity
Bridge	zeroGradient	epsilonWall-Function	kqRWall-Function	nutkWall-Function	omegaWall-Function	fixedFlux-Pressure	noSlip



282  
 283 **Figure 5. OpenFOAM Model Geometry and Boundary Conditions**

284 **3.1 Structural analysis and damage assessment**

285 The *OpenSees* model was developed using fiber-based line elements for the reinforced-concrete pier columns and preflex  
 286 girders (a form of prestressed, concrete-encased steel beams). Nonlinear concrete (Concrete02) and steel (Steel02) constitutive  
 287 models were employed to simulate uniaxial material response in the fibers. All concrete was assumed to have a compressive  
 288 strength of 34.5 MPa. The steel reinforcement and encased structural steel was assumed to have yield stresses of 276 MPa and  
 289 379 MPa, respectively. The girders ends were connected to pier caps (modeled as rigid) via linear-elastic springs to represent  
 290 bearings. The free spherical bearings were modeled as roller boundary conditions. The steel-laminated elastomeric bearing  
 291 pads were modeled with lateral, vertical, rotational, and torsional stiffnesses based on linear theory of bearings as described  
 292 by Stanton et al. (2008). The elastomeric bearing dimensions are shown in Figure 4; each had two, 13-mm-thick layers of  
 293 elastomer reinforced with 3-mm steel plates. The elastomer was assumed to have a bulk modulus of 3100 MPa and a shear  
 294 modulus of 0.76 MPa; the bearing dimensions and material properties led to the stiffness parameters defined in Table 4. The  
 295 bearing spring elements were connected to rigid links which simulated pier cap beams, providing a load path between the  
 296 girders and pier columns. The bridge abutments were founded on rock on the north side and piles on the south side; both  
 297 abutments were modeled as rigid. The piers were founded on rock and pier columns were modeled as fixed. It is noted that  
 298 many bridge foundations are vulnerable to scour, especially under flood conditions; however, scour and soil-structure  
 299 interaction effects are beyond the scope of the present work.

300 **Table 4.** *OpenSees* Elastomeric Bearing Spring Stiffnesses

Stiffness type	Direction	Value
Axial	—	142 kN/mm
Shear	—	1.69 kN/mm
Rotational	Deformation in short-axis direction	311 kN-m/rad
	Deformation in long-axis direction	2350 kN-m/rad
Torsional	—	17.9 kN-m/rad

301

302 To analyze the bridge, gravity loads were first applied based on the self-weight of the structural components; no live loads  
 303 were considered. The lateral forces, vertical forces, and roll moments determined from *OpenFOAM* were then applied as  
 304 distributed loads in *OpenSees* on each bridge girder (i.e., over all eight spans with 20 girders per span); this is the key link  
 305 between the CFD and structural models.

306 Under the range of loading investigated, yielding or cracking was not detected in the girders or columns, and the simulated  
 307 hydraulic forces were not large enough to overcome the self-weight of the structure, which would result in uplift of the  
 308 superstructure. However, the elastomeric bearing pads sustained large shear demands near the design limits specified by  
 309 Section 14.7.5 of the AASHTO *LRFD Bridge Specification* (2017). Specifically, the elastomeric bearings were evaluated for:

- 310 i. loss of frictional resistance between the bearing and girder based on the ratio of shear and normal forces on the
- 311 bearings,
- 312 ii. excessive shear deformation, and
- 313 iii. excessive shear strain due to combined axial load, rotation, and shear deformation.

314 The solid lines in Figure 6 compare maximum shear forces, deformations, and strains in any of the elastomeric bearings for  
 315 each of the loading scenarios investigated; Figures 6a, 6c, and 6e show these engineering demand parameters versus flow  
 316 velocity and Figures 6b, 6d, and 6f show corresponding values with respect to flow height. The data suggest that peak steady-  
 317 state demands on any of the elastomeric bearings in the bridge occur around a flow height 15 m, at which point the bridge has  
 318 just reached full inundation. In addition, below a flow height of 15 m, demands consistently increase with velocity; such  
 319 increases in demand after full inundation are not consistently observed, which suggests that the loading is primarily associated  
 320 with hydrodynamic effects that are a function of the effective area of the cross-section, and may also be affected by the fact  
 321 that the flow around the superstructure is less turbulent. To expand the data set, linear extrapolation to flow velocities of up to  
 322 6 m/s are shown in Figures 6a, 6c, and 6e as dotted lines with open markers. It is noted that the plots in Figure 6 show peak  
 323 demands across all elastomeric bearings in the bridge, and the actual extent of damage depends on the progression of failure  
 324 in multiple bearings.

325 The Commentary to the AASHTO *LRFD Bridge Specification* (2017) states a coefficient of friction of 0.2 between elastomeric  
 326 bearings and concrete is appropriate for design, and this limit is used here to evaluate potential girder unseating due to loss of  
 327 frictional resistance. For the purpose of this evaluation, dowel resistance is neglected, though this could prevent unseating in  
 328 practice. Figures 6a and 6b plot the peak ratios of shear-to-normal forces across all bearings on the bridge, and it can be  
 329 observed that the bearings are well below the limit suggested in the AASHTO Commentary, which is labeled as  $\mu_{max}$  and  
 330 shown as the grey line. However, it must be noted that the coefficient of friction may be lower than expected under wet  
 331 conditions and that the lateral hydrodynamic loading can be significant, increasing vulnerability of unseating due to debris  
 332 impact. Conservatively considering a reduced coefficient friction of 0.1, the results indicate flow conditions for which the  
 333 frictional resistance is approached or exceeded: 13.5-m flow depth with velocity of at least 6 m/s, 15-m flow depth with  
 334 velocity of at least 5 m/s, 18-m flow depth with velocity of at least 6 m/s.

335 Figures 6c and 6d show peak shear strains due to loading perpendicular to the short edge of the bearing pad (see Figure 4b)  
 336 due to combined axial load ( $\gamma_a$ ), rotation ( $\gamma_r$ ), and shear ( $\gamma_s$ ). The shear strains are computed based on Eqs. 4-6 based on the  
 337 AASHTO *LRFD Bridge Specification* (2017).

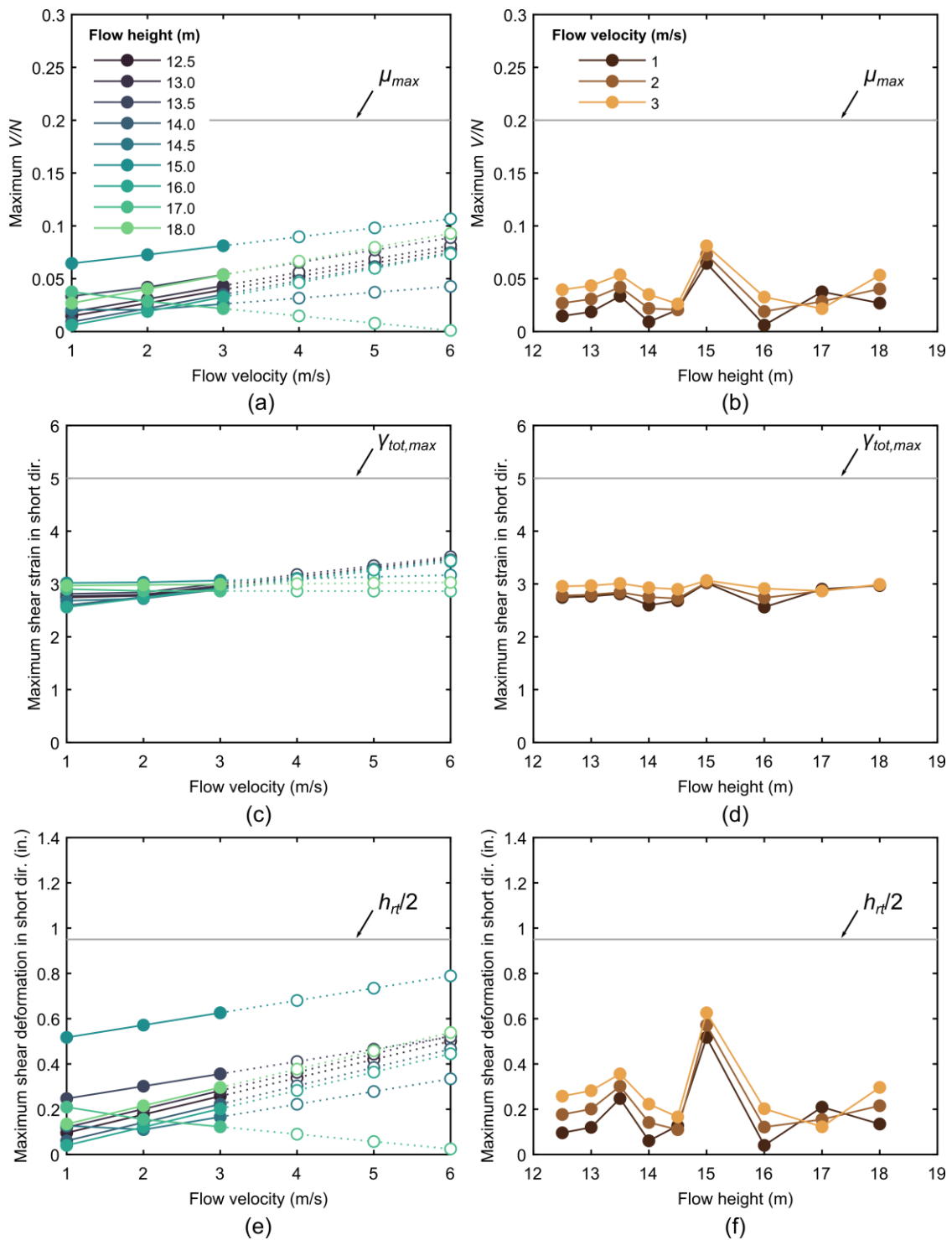
$$\gamma_a = D_a \frac{\sigma_s}{G S_i} \quad \text{Eq. 4}$$

$$\gamma_r = D_r \left( \frac{L}{h_{ri}} \right)^2 \frac{\theta_s}{n} \quad \text{Eq. 5}$$

$$\gamma_s = \frac{\Delta_s}{h_{rt}} \quad \text{Eq. 6}$$

338 In the above equations,  $D_a$  and  $D_r$  are empirical coefficients,  $\sigma_s$  is the average compressive stress,  $G$  is the shear modulus,  $S_i$   
 339 is the shape factor of the  $i$ th internal layer,  $L$  is the bearing length perpendicular to the axis of rotation,  $h_{ri}$  is the thickness of  
 340 the  $i$ th internal elastomeric layer,  $h_{rt}$  is the total thickness of the elastomer,  $\theta_s$  is the rotation demand,  $n$  is the number of interior  
 341 elastomeric layers, and  $\Delta_s$  is the shear deformation. Note that  $\sigma_s$ ,  $\theta_s$ , and  $\Delta_s$  are outputs from the structural analysis; the  
 342 rotation demand,  $\theta_s$ , includes 0.005 rad of rotation due to misalignment. For design per the AASHTO *LRFD Bridge*  
 343 *Specification* (2017), the combined shear strain due to these actions should not exceed 5.0, and this criterion is satisfied in the  
 344 analyses (all values, including extrapolated values, are below the grey line in Figures 6c and 6d).

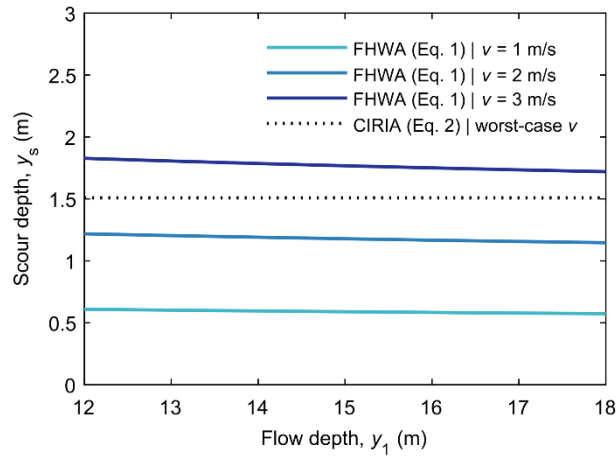
345 The shear deformation demand on the bearing,  $\Delta_s$ , is shown to be more critical than the combined shear strains: Figures 6e  
 346 and 6f show these data with the annotated shear strain limit of  $h_{rt}/2$  in grey; this limited is also based on the AASHTO  
 347 *Specification* (2017). The demand is clearly largest for a flow height of 15 m, and it increases linearly with the flow velocity.



348

349 **Figure 6. Simulated demand on elastomeric bearings in M6 bridge evaluated for various limit states; (c) and (d) show peak shear**  
 350 **strains on the short edge of the bearing pad, due to combined axial load, moment, and shear.**

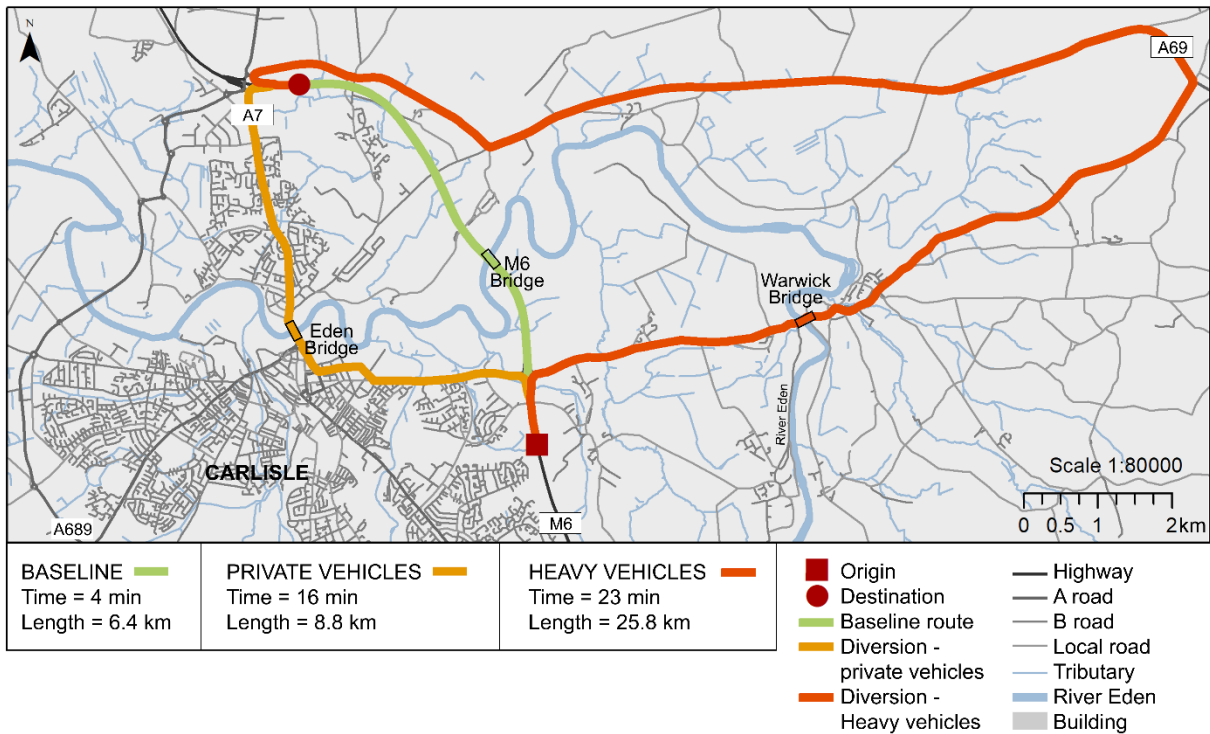
351 Scour is also a concern for many riverine bridges, and an example evaluation based on the M6 bridge is shown here using the  
 352 HEC-18 (Arneson et al., 2012) and CIRIA scour equations (Kirby et al., 2015; HE, 2012). Figure 7 shows estimated scour  
 353 depths at the bridge piers for worst-case assumptions for soil (i.e. highly mobile soil). For both methods, there is little or no  
 354 variation with flow depth due to the tall, narrow geometry of the piers. Although the CIRIA scour equation is independent of  
 355 flow velocity, when the flow velocity exceeds the soil threshold velocity (case shown in Figure 7), its scour depth estimates  
 356 resulted similar to the FHWA equation for flow velocity between 2 and 3 m/s. Scour depths in this range (i.e. between 1 and  
 357 2 m) would likely result in significantly altered foundational restraint and therefore require more sophisticated fluid-soil-  
 358 structure interaction modelling. Explicit scour modelling was beyond the scope of this work.



359  
 360 **Figure 7. Scour depth for Eden Bridge using FHWA equation (blue lines) and CIRIA equation (dotted line).**

361 **3.2 Network impact and consequence assessment**

362 The results of the loosely coupled CFD and structural analyses described above suggest a potential for either girder unseating  
 363 due to loss of frictional resistance or excessive shear deformation, which may lead to debonding and delamination for this  
 364 particular bridge. In addition, damage associated with these limit states is most expected at a flow height of 15 m and flow  
 365 velocity of at least 5 m/s. The impact of damage in this flood scenario is therefore considered in this section. Based on Table  
 366 1, the damage state is estimated as moderate because: (i) the bearings approach but do not exceed limit states, (ii) scour is  
 367 assumed to be insignificant compared to damage to the superstructure and bearings, and (iii) water overtops the bridge deck.  
 368 A moderate damage state implies the bridge closure for 5-12 days (see Table 1). In the case of the M6 bridge, its closure causes  
 369 disruptions to all southbound and northbound users that are travelling along the M6 (Figure 8). Compared to the baseline  
 370 journey, results show that private cars are delayed by 12 minutes and have additional ca. 9 km due to rerouting. HGVs cannot  
 371 travel via the historic Eden Bridge (city center) and are subjected to a longer rerouting, which leads to 19 minutes and ca. 20  
 372 km of delay and additional travelling respectively.



373  
 374 **Figure 8. Routes for crossing the river Eden along the highway in baseline and disrupted conditions; private and heavy vehicles are**  
 375 **rerouted on different journeys when the M6 bridge is disrupted.**

376 The cost of the impact due to the M6 bridge disruption is computed in terms of direct and indirect consequences using Eq. 1;  
 377 output and input values are specified in Table 5.

378 **Table 5. Output and input data for the impact cost calculation considering disruption due to an extreme flood event on the M6**  
 379 **bridge in Carlisle. Acronyms: VTT – Value of Travel Time; HGV - Heavy Good Vehicle; VOC – Vehicle Operating Cost; ADT -**  
 380 **Average Daily Traffic.**

	VARIABLE	DATA	SOURCE
INPUT	Average repair cost (£/m <sup>2</sup> )	£36.54/m <sup>2</sup>	Table 1
	Time for repairs ( $T_{repair}$ )	7 days	Table 1
	VTT for HGVs	£10.10/hour	DfT (2009)
	Delay for HGVs	19 min	computed
	Detour length for HGVs	19.4km	computed
	VOC for HGVs	37.668 p/km	Blakemore (2018)
	ADT for HGVs	1833 veh/day	UK national statistics
	VTT for average private vehicles	£6.81/hour	DfT (2009)
	Delay for average private vehicles	12 min	computed
	Detour length for private vehicles	2.4 km	computed
	VOC for private vehicles	25.47p/km	Yurday (2020)
	ADT for average private vehicles	28602 veh/day	UK national statistics
OUTPUT	$C_{repair}$	£7,308.00	computed
	$C_{clean}$	£29,476.00	Panici et al. (2020)
	$C_{detour}$	£30,878.65/day	computed
	$C_{delay}$	£44,818.47/day	computed
TOTAL		£566,663.81	

381  
 382 The values of Value of Travel Time (VTT) of HGVs (Heavy Good Vehicles, working condition) and average private cars  
 383 (unspecified conditions) can be found in the UK Department for Transport (DfT) appraisal methods, illustrated in the Cost  
 384 Benefit Analysis (COBA) manual (DfT, 2009). Data regarding the additional travel time for rerouting has been computing via  
 385 transport model (Sec. 2.5) and verified with Google Maps (Figure 8); for the UK, topological road network links are freely  
 386 available nationwide. Data regarding Average Daily Traffic (ADT) flow are freely available  
 387 (<http://webtris.highwaysengland.co.uk/>) and were obtained by considering the annual northbound and southbound flows for  
 388 the relevant sites (36,670 veh/day: Site 9538/2 on link M6 southbound and Site 9540/2 on link M6 northbound; 2019 data),  
 389 considering the traffic composition at 78% for private cars and 5% for HGVs (DfT, 2019).

390 The repair cost ( $C_{repair}$ ) was computed using Table 1 and assuming 7 days (average) of bridge closure; the cost of debris  
 391 removal was obtained by looking at the highest cost for a single event in the UK (Panici et al., 2020), since the simulated  
 392 flooding is an extreme and rare event. The additional vehicle operating due to the detour per day ( $C_{detour}$ ) was calculated using  
 393 Eq. 2; the cost associated with trip delays ( $C_{delay}$ ) was calculated using Eq. 3.

394 For the case study undertaken (Carlisle, UK; 1-in-a-500-ys event), the total cost of the flood impact to the bridge is  
 395 £566,663.81, considering seven days of bridge closure. The largest proportion (93.5%) of this cost is due to the indirect cost  
 396 of rerouting traffic (£75,697.12 per day of closure, i.e. £529,879.81); the 6.5% of the total cost is due to direct damages only  
 397 (£36,784.00).



399 This study developed an integrated method that uses a multiphysics, multilevel approach for assessing the effect of flooding  
400 hazards on a local transportation network. For the City of Carlisle (UK), a 1-in-500-years flooding event was simulated and  
401 the resulting hydrodynamic forces on the highway bridge (M6) modelled. While simulated hydrodynamic forces and Finite  
402 Element (FE) analysis did not show uplift failure, overtopping of the bridge is shown to occur at inundation heights of 14 m  
403 and above. Given the potential for flood-water disruption of traffic, overtopping should be considered temporary network  
404 failure in its own right. The elastomeric bearings supporting the bridge girders approached shear deformations near design  
405 limits at a flow height of 15 m, and a potential loss of frictional resistance between the elastomer and concrete is also observed.  
406 While these limit states were not exceeded for flow velocities up to 3 m/s, extrapolation to faster flow rates suggests higher  
407 potential for damage. This notwithstanding, the bridge would lose immediate functionality at a flow height of between 13.5  
408 and 14.0 m due to inundation of the deck even if the structure sustains no damage. The impact analysis showed that indirect  
409 damages covered the 93.5% of the total cost of damages to the bridge, proving that limiting the assessment to repairs and  
410 debris cleaning would greatly underestimate the impact of flooding to bridges.

411 The produced outputs are conceptual results and thus approximate and indicative for multiple reasons. First, there is a dearth  
412 of UK-specific data regarding bridge repairs, duration time of repair, etc.; research or survey to solicit post-flood data are  
413 highly recommended to improve impact estimates. For example, a bridge could be partially closed during repairs (according  
414 to its damage state) and allow traffic in one direction. Second, the modeling approach presented herein used several intentional  
415 simplifications for demonstration purposes, including reducing the CFD domain, neglecting soil-foundation effects and scour  
416 modeling, and assumed rigidity of the structural system among others. In scenarios where these issues (or others) may be of  
417 more concern for a particular bridge, the fidelity of the modeling approach could be improved. Additionally, the failure states  
418 presented here may not translate broadly to the general bridge inventory, but additional or alternative structural/functional  
419 failure states could be applied. Third, the impact analysis was limited to private cars and HGVs for demonstration purposes;  
420 however, advanced transport appraisal could better capture users' choices and the engineering response of lifelines by  
421 including a wider range of vehicles categories and traffic scenarios. In terms of impact, the presence of floodwater on the roads  
422 is not simulated for limiting the focus of this work on riverine flooding and the bridge impact consequences; for properly  
423 analyzing the flooding impact to road networks, simulation of surface water flooding should be undertaken; this analysis would  
424 be a study on its own, and currently out of the scope of this piece of research. Flood impact on other parts of the network would  
425 limit the capacity of the alternative routes, causing additional delays to the traffic; thus, obtained results represent an  
426 underestimation of the overall systemic cost. Nevertheless, the proposed approach of impact analysis can give community  
427 leaders a robust method for assessing susceptibility to flooding and relative consequences at systemic level and the case study  
428 presented here represents an archetype for this approach.

429 Thus, the importance of this study consists in the proof of concept of a new holistic methodology using a multilevel approach  
430 to improve the fidelity of network failure predictions. The computed hydrodynamic forces were applied directly into a  
431 traditional FE model to predict the global structural response to identify critical structural components and damage states.  
432 Notably, the hydrodynamic forces induced large demands on bearings that are often not considered in design. Because of the  
433 critical nature of bridges to a transportation network, the impact analysis revealed that indirect cost cover almost all the total  
434 cost due to flooding; this consideration is fundamental for infrastructure owners and managers when managing assets and  
435 budgets.

436 Next steps of this study will analyze the impact of the closure for a portfolio of bridges, in isolation and any combination of  
437 them. Future work should investigate the impacts of other limit states which could result in total or partial bridge closure; a  
438 wider range of bridge types should be investigated too. Such analyses would benefit from 3D CFD and FE models to help  
439 refining demands on the structure and reducing uncertainty in the predicted bridge performance. Ultimately, this approach can  
440 be applied to any coastal or riverine structure where large-scale water inundation is expected.

## 441 **5 CONCLUSION**

442 This study focused on riverine bridges prone to failures during flood events. This study established rigorous practices of  
443 Computational Fluid Dynamics (CFD) for modelling hydrodynamic forces on inundated bridges, and understanding the  
444 consequences of such impact on the surrounding network. The hydrodynamic forces were modelled as demand on the bridge  
445 structure and inputted into a vulnerability analysis of the structure; the performance evaluation s showed a moderate damage  
446 state of the bridge which was used to approximate the overall direct and indirect consequences. For the City of Carlisle (UK)  
447 and a 1-in-500-years flooding, results showed that the flood impact to the M6 bridge (highway bridge) caused more than £500k  
448 of damages of which 93.5% indirect damages (rerouting and delays). The relevance of this work resides in the integrated  
449 method that couple practices of CFD with performance and network analysis, which allows to estimate the cost due to flooding  
450 impact to a bridge considering the surrounding transport system. Infrastructure owners and managers, as well as modelers and  
451 researchers, should build on this work to better predict local fluid pressures that may lead to bridge structural failure and related  
452 network economic consequences.

## 453 **DATA AVAILABILITY STATEMENT**

454 All relevant and publicly available data will be shared via the DataBris repository of the University of Bristol if the paper will  
455 be accepted for publication; data sources are clearly specified throughout the paper.

## 456 **ACKNOWLEDGEMENTS**

457 MP was supported by the Engineering and Physical Sciences Research Council (EPSRC) LWEC (Living With Environmental  
458 Change) Fellowship (EP/R00742X/1 and 2). The authors also grateful acknowledge: Mark Pooley at Highways England; John  
459 L. Kelsall at Phoenix Architecture & Planning; Mohammad Fereshtehpour at Ferdowsi University of Mashhad.

## 460 **References**

- 461 AASHTO: Standard specifications for highway bridges, 7<sup>th</sup> Edition, Washington, DC, 2002.
- 462 AASHTO: AASHTO LRFD Bridge Design Specifications; 8<sup>th</sup> Edition, Washington, DC, 2017.
- 463 Ahamed, T., Duan, J. G., Jo, H.: Flood-fragility analysis of instream bridges—consideration of flow hydraulics, geotechnical  
464 uncertainties, and variable scour depth. *Structure and Infrastructure Engineering*, 1-14, 2020.
- 465 Argyroudis, S.A., Mitoulis, S.A., Winter, M.G., Kaynia A.M.: Fragility of transport assets exposed to multiple hazards: State-  
466 of-the-art review toward infrastructural resilience, *Reliability Engineering & System Safety* 191, 106567,  
467 <https://doi.org/10.1016/j.res.2019.106567>, 2019.
- 468 Arneson, L.A., Zevenbergen, L.W., Lagasse P.F., Clopper, P.E.: Evaluating scour at bridges, 5<sup>th</sup> Edition, Publication no.  
469 FHWA-HIF-12-003, Hydraulic Engineering Circular No. 18. U.S. Department of Transportation, Federal Highway  
470 Administration, 2012.
- 471 Arrighi C., Pregnolato M., Dawson R., Castelli F.: Preparedness against mobility disruption by floods, *Science of the Total*  
472 *Env.*, 654: 1010-1022, <https://doi.org/10.1016/j.scitotenv.2018.11.191>, 2019.
- 473 Bates P.D., Horritt M.S. and Fewtrell T.J.: A simple inertial formulation of the shallow water equations for efficient two-  
474 dimensional flood inundation modelling, *J. Hydrol.* 387(1–2): 33-45. doi: 10.1016/j.jhydrol.2010.03.027, 2010.
- 475 Blakemore T.: Truck operating costs report for 2018: <https://thetruckexpert.co.uk/truck-operating-costs-report-for-2018/> last  
476 access: 12 May 2020, 2018.

477 Carey T.J., Mason H.B., Barbosa A.R., Michael H.S.: Multihazard Earthquake and Tsunami Effects on Soil–Foundation–  
478 Bridge Systems, *J. Bridge Eng.*, 24(4), 04019004, doi: [https://doi.org/10.1061/\(ASCE\)BE.1943-5592.0001353](https://doi.org/10.1061/(ASCE)BE.1943-5592.0001353), 2019

479 Department for Transport (DfT): COBA Manual: [https://www.gov.uk/government/publications/cobalt-software-and-user-](https://www.gov.uk/government/publications/cobalt-software-and-user-manuals)  
480 [manuals](https://www.gov.uk/government/publications/cobalt-software-and-user-manuals), last access: 12 May 2020, 2009.

481 Department for Transport (DfT): Road Traffic Estimates: Great Britain 2018:  
482 [https://assets.publishing.service.gov.uk/government/uploads/system/uploads/attachment\\_data/file/808555/road-traffic-](https://assets.publishing.service.gov.uk/government/uploads/system/uploads/attachment_data/file/808555/road-traffic-estimates-in-great-britain-2018.pdf)  
483 [estimates-in-great-britain-2018.pdf](https://assets.publishing.service.gov.uk/government/uploads/system/uploads/attachment_data/file/808555/road-traffic-estimates-in-great-britain-2018.pdf), last access: 12 May 2020, 2019.

484 de Almeida G.A.M., Bates P.D., Freer J.E., Souvignet M.: Improving the stability of a simple formulation of the shallow water  
485 equations for 2-D flood modelling, *Water Resour. Res.*, 48(5), W05528, doi: 10.1029/2011wr011570, 2012.

486 EA: Carlisle Flood Investigation Report 2016. Environment Agency (EA), Cumbria County Council:  
487 <https://www.cumbria.gov.uk/planning-environment/flooding/flood-investigation-reports-carlisle.asp>, last access: 12  
488 November 2020, 2016.

489 Ertugay K., Argyroudis S. and Düzgün H.Ş.: Accessibility modeling in earthquake case considering road closure probabilities:  
490 a case study of health and shelter service accessibility in Thessaloniki, Greece, *Int. J. of Disaster Risk Reduction*, 17, 49–  
491 66, <https://doi.org/10.1016/j.ijdr.2016.03.005>, 2016.

492 Gardoni, P.: *Routledge Handbook of Sustainable and Resilient Infrastructure*. London, Routledge,  
493 <https://doi.org/10.4324/9781315142074>, 2018.

494 Gidaris, I., Padgett, J. E., Barbosa, A. R., Chen, S., Cox, D. T., Webb, B. and Cerato, A.: Multiple-hazard fragility and  
495 restoration models of highway bridges for regional risk and resilience assessment in the United States: State-of-the-art  
496 review, *J. Struct. Eng.* 143 (3), 04016188, [https://doi.org/10.1061/\(ASCE\)ST.1943-541X.0001672](https://doi.org/10.1061/(ASCE)ST.1943-541X.0001672), 2017.

497 Gehl, P. and D’Ayala, D.: System loss assessment of bridge networks accounting for multi-hazard interactions. *Structure and*  
498 *Infrastructure Engineering*, 14(10), 1355-1371, 2018.

499 Grossi, P. and Kunreuther, H.: *Catastrophe Modeling: A New Approach to Managing Risk*, New York, Springer-Verlag, 2005.

500 FEMA: HAZUS-MH MR1: Technical manual, Earthquake Model, Federal Emergency Management Agency, Washington,  
501 D.C., 2003.

502 Highways England (HE): Design Manual for Roads and Bridges BD 97/12 The assessment of scour and other hydraulic actions  
503 at highway structures: <http://www.standardsforhighways.co.uk/ha/standards/dmrb/vol3/section4/bd9712.pdf>, last access:  
504 12 May 2020, 2012.

505 Hung, C. C., Yau, W. G.: Vulnerability evaluation of scoured bridges under floods. *Engineering Structures*, 132, 288-299,  
506 2017.

507 Kerenyi, K., Sofu, T. and Guo: J. Hydrodynamic forces on inundated bridge decks, Federal Highway Administration, FHWA-  
508 HRT-09-028, 2009.

509 Kilanitis, I. and Sextos, A.: Integrated seismic risk and resilience assessment of roadway networks in earthquake prone areas,  
510 *Bulletin of Earthquake*, 17, 181–210, <https://doi.org/10.1007/s10518-018-0457-y>, 2019.

511 Kim, H., Sim, S. H., Lee, J., Lee, Y. J., Kim, J. M.: Flood fragility analysis for bridges with multiple failure modes. *Advances*  
512 *in Mechanical Engineering*, 9(3), 1687814017696415, 2017.

513 Kirby, A. M., Roca, M., Kitchen, A., Escarameia, M. and Chesterton, O. J.: *Manual on scour at bridges and other hydraulic*  
514 *structures*, 2<sup>nd</sup> edition, CIRIA C742, RP987, London, CIRIA, ISBN: 978-0-86017-747-0, 2015.

515 Lam, J. C. and Adey, B. T.: Integrating functional loss assessment and restoration analysis in the quantification of indirect  
516 consequences of natural hazards, *ASCE-ASME J. Risk and Uncertainty in Eng. Systems, Part A: Civil Engineering*, 2:  
517 04016008, <https://doi.org/10.1061/AJRU6.0000877>, 2016.

518 Liu, L., Frangopol, D.M., Mondoro, A. and Yang, D.Y.: Sustainability-Informed Bridge Ranking under Scour Based on  
519 Transportation Network Performance and Multi-attribute Utility. *J. Bridge Eng.*, 23(10), 04018082,  
520 [https://doi.org/10.1061/\(ASCE\)BE.1943-5592.0001296](https://doi.org/10.1061/(ASCE)BE.1943-5592.0001296), 2018.

521 Lomonaco, P., Alam M. S., Arduino, P., Barbosa, A., Cox, D.T., Do, T., Eberhard, M., Motley, M.R., Shekhar, K., Tomiczek,  
522 T., Park, H., van de Lindt, J.W. and Winter, A.: Experimental modeling of wave forces and hydrodynamics on elevated  
523 coastal structures subject to waves, surge or tsunamis: the effect of breaking, shielding and debris, *Coastal Eng. Proceedings*  
524 1 (36), 53, <https://doi.org/10.9753/icce.v36.waves.53>, 2018.

525 McKenna, F., Scott, M.H., and Fenves, G.L.: Nonlinear finite-element analysis software architecture using object composition,  
526 *J. Comput. Civ. Eng.* 24: 95-107, 2010.

527 Mondoro, A. and Frangopol, D.M.: Risk-based cost-benefit analysis for the retrofit of bridges exposed to extreme hydrologic  
528 events considering multiple failure modes, *Eng. Struct.*, 159, 310-319, <https://doi.org/10.1016/j.engstruct.2017.12.029>,  
529 2018.

530 Motley, M.R., Wong, H.K., Qin X., Winter, A.O. and Eberhard, M.O.: Tsunami-induced forces on skewed bridges, *J.*  
531 *Waterway, Port, Coastal, Ocean Eng.* 142(3), 04015025, [https://doi.org/10.1061/\(ASCE\)WW.1943-5460.0000328](https://doi.org/10.1061/(ASCE)WW.1943-5460.0000328), 2016.

532 Neal, J.C., Bates, P.D., Fewtrell, T.J., Hunter, N.M., Wilson, M.D. and Horritt, M.S.: Distributed whole city water level  
533 measurements from the Carlisle 2005 urban flood event and comparison with hydraulic model simulations, *J. Hydrol.*,  
534 368(1-4), 42-55, <https://doi.org/10.1016/j.jhydrol.2009.01.026>, 2009.

535 Neal, J.C, Dunne, T., Sampson, C., Smith, A. and Bates, P.D.: Optimisation of the two-dimensional hydraulic model  
536 LISFLOOD-LP for CPU architecture, *Environ. Model. Softw.*, 107, 148-157,  
537 <https://doi.org/10.1016/j.envsoft.2018.05.011>, 2018

538 Oudenbroek, K., Naderi, N., Bricker, J.D., Yang, Y., Van der Veen, C., Uijttewaal, W., Moriguchi, S. and Jonkman, S.N.:  
539 Hydrodynamic and Debris-Damming Failure of Bridge Decks and Piers in Steady Flow, *Geosciences*, 8 (11), 409,  
540 <https://doi.org/10.3390/geosciences8110409>, 2018..

541 Padgett, J.E., DesRoches, R., Nielson, B., Yashinsky, M., Kwon, O.-S., Burdette, M. and Tavera E.: Bridge damage and repair  
542 costs from hurricane Katrina, *J. Bridge Eng.*, 13(1), 6-14, [https://doi.org/10.1061/\(ASCE\)1084-0702\(2008\)13:1\(6\)](https://doi.org/10.1061/(ASCE)1084-0702(2008)13:1(6)), 2008.

543 Panici, D., Kripakaran, P., Djordjević, S. and Dentith, K.: A practical method to assess risks from large wood debris  
544 accumulations at bridge piers, *Science of The Total Environment*, 728, 138575,  
545 <https://doi.org/10.1016/j.scitotenv.2020.138575>, 2020

546 Pregnotato, M., Vardanega, P.J., Limongelli, M. P., Giordano, P. F. and Prendergast, L. J. Risk-based scour management: a  
547 survey, In: *Bridge Maintenance, Safety, Management, Life-Cycle Sustainability and Innovations: Proceedings of the 10<sup>th</sup>*  
548 *International Conference on Bridge Maintenance, Safety and Management (IABMAS 2020)*, Sapporo, Japan, 11-15 April  
549 2021 (Yokota, H. & Frangopol, D.M. (eds.)). CRC Press/Balkema Taylor & Francis Group, The Netherlands, pp. 1258-  
550 1264. <https://doi.org/10.1201/9780429279119-170>, 2021a.

551 Pregnotato, M., Winter, A.O., Mascarenas, D., Sen, A.D., Bates, P. and Motley, M.R.: An integrated impact analysis for  
552 riverine bridges subjected to high river flows, In: *Bridge Maintenance, Safety, Management, Life-Cycle Sustainability and*  
553 *Innovations: Proceedings of the 10<sup>th</sup> International Conference on Bridge Maintenance, Safety and Management (IABMAS*  
554 *2020)*, Sapporo, Japan, 11-15 April 2021 (Yokota, H. & Frangopol, D.M. (eds.)). CRC Press/Balkema Taylor & Francis  
555 Group, The Netherlands, pp. 693-701. <https://doi.org/10.1201/9780429279119-91>, 2021b.

556 Pregnotato, M.: Bridge safety is not for granted – A novel approach for bridge management, *Eng. Structures*, 196, 109193,  
557 <https://doi.org/10.1016/j.engstruct.2019.05.035>, 2019.

558 Pregnotato M., Ford A., Robson C., Glenis V., Barr, S. and Dawson R.J.: Assessing Urban Strategies for Reducing the Impacts  
559 of extreme Weather on Infrastructure Networks, *Royal Soc. Open Sci.*, 3(5), 1-15, doi: 10.1098/rsos.160023, 2016.

560 Qin, X., Motley, M.R. and Marafi, N.: Three-dimensional modeling of tsunami forces on coastal communities, *Coast. Eng.*,  
561 140, 43–59, <https://doi.org/10.1016/j.coastaleng.2018.06.008>, 2018.

562 Solomon, S., Manning, M., Marquis, M. and Qin, D.: *Climate change 2007 - the physical science basis: Working group I*  
563 *contribution to the 4<sup>th</sup> assessment report of the IPCC*, Cambridge University Press, Cambridge, 2007.

564 Stanton, J. F., Roeder, C. W., Mackenzie-Helnwein, P., White, C., Kuester, C., and Craig, B.: *Rotation Limits for Elastomeric*  
565 *Bearings*, NCHRP Report 596, The National Academies Press, Washington D.C., doi: 10.17226/23131, 2008.

566 Stephens, M.T., Winter, A., Motley, M.R., and Lehman, D.E.: Comparing seismic and tsunami load demands on reinforced  
567 concrete and concrete filled steel tube bridges, *Proceedings of the 39<sup>th</sup> IABSE Symposium*, 2017.

568 Tryggvason, G., Scardovelli, R. and Zaleski, S.: *Direct numerical simulations of gas–liquid multiphase flows*, Cambridge  
569 University Press, Cambridge, 2011.

570 Yang, D. Y. and Frangopol, D.: Life-cycle management of deteriorating bridge networks with network-level risk bounds and  
571 system reliability analysis, *Struct. Safety*, 83, 101911, <https://doi.org/10.1016/j.strusafe.2019.101911>, 2020.

572 Yilmaz, T., Banerjee, S. and Johnson, P. A.: Performance of two real-life California bridges under regional natural hazards. *J.*  
573 *Bridge. Eng.* 21(3), 1–15, [https://doi.org/10.1061/\(ASCE\)BE.1943-5592.0000827](https://doi.org/10.1061/(ASCE)BE.1943-5592.0000827), 2016.

574 Yurday, E.: Average Cost to Run a Car UK 2020: <https://www.nimblefins.co.uk/average-cost-run-car-uk>, last access: 12 May  
575 2020, 2020.

576 Wang, C., Yu, X. and Liang, F.: A review of bridge scour: mechanism, estimation, monitoring and countermeasures, *Nat.*  
577 *Hazards*, 87, 1881–1906, <https://doi.org/10.1007/s11069-017-2842-2>, 2017.

578 Wardhana, K. and Hadipriono, F. C.: Analysis of Recent Bridge Failures in the United States, *J. Perf. of Constructed Facilities*  
579 17(3), 144–150, [https://doi.org/10.1061/\(ASCE\)0887-3828\(2003\)17:3\(144\)](https://doi.org/10.1061/(ASCE)0887-3828(2003)17:3(144)), 2003.

580 Werner, S. D., Cho, S. and Eguchi, R. T.: *The ShakeOut Scenario Supplemental Study: Analysis of Risks to Southern*  
581 *California Highway System*, SPA Risk LLC, Denver, CO, 2008.

582 Winter, A.O., Motley M.R. and Eberhard M.O.: Tsunami-like wave loading of individual bridge components, *J. Bridge Eng.*  
583 23 (2), 04017137, [https://doi.org/10.1061/\(ASCE\)BE.1943-5592.0001177](https://doi.org/10.1061/(ASCE)BE.1943-5592.0001177), 2017.

584 Zhou, Y., Banerjee, S. and Shinozuka, M.: Socio-economic effect of seismic retrofit of bridges for highway transportation  
585 networks: a pilot study, *Struct. Infrastruct. Eng.* 6, 145-157, <https://doi.org/10.1080/15732470802663862>, 2010